ERJ
Engineering Research Journal
Faculty of Engineering
Minoufiya University

# A STABLE ADAPTIVE FLUX OBSERVER FOR A VERY LOW SPEED-SENSORLESS INDUCTION MOTOR DRIVES INSENSITIVE TO STATOR RESISTANCE VARIATIONS

**Mohamed S. Zaky**

*Electrical Engineering Department, Faculty of Engineering, Minoufiya University, Shebin El-Kom, Egypt*

**ABSTRACT**

In recent years, numerous attempts have been made to improve the performance of speed-sensorless induction motor drives. Adaptive flux observer (AFO) is one of the machine model based methods of speed estimation. Parameter variations, low-speed operation and the difficulty encountered in the design of the feedback gain and the adaptation mechanism are the most critical aspects affecting the accuracy and stability of this method. In this paper, design of the observer feedback gain is proposed to ensure the stability over a wide range of operation especially in the low-speed region. The characteristic equation of the closed loop speed estimator is derived. The values of the adaptive law parameters corresponding to the marginal system stability are determined based on Routh-Hurwitz criterion. The sensitivity of AFO to stator resistance mismatch is studied. A stator resistance adaptation scheme for accurate speed estimation at low speeds is derived using Popov's hyper-stability theory. The relation between the identification error of the rotor speed and adaptive gains is clarified. An experimental setup based on a DSP system is implemented. The simulation and experimental results confirm the efficacy of the proposed approach.

أجريت في الآونة الأخيرة محاولات عديدة لضمان خصائص أداء عالية لنظم تسيير المحرك التأثيرى التى تعمل بطرق التحسس والاستشعار غير المباشر للسرعة بدلا من القياس المباشر لها. ومن الطرق التي تستخدم مع الأنظمة غير الخطية – مثل منظومة المحرك التأثيري– تلك الطريقة التي تعتمد على مراقب الفيض التكيفى وهى تصنف ضمن الطرق التي تعتمد بصفة أساسية على معاملات الآلة في حساب السرعة. ويعتبر تغير معاملات الآلة والسرعات المنخفضة والصعوبات فى اختيار كسب كل من التغذية الاسترجاعية وآلية التكيف من أهم العوامل التى تؤثر على دقة واستقرار هذا النوع من المراقبات. ويقترح هذا البحث تصميم كسب التغذية الاسترجاعية لضمان استقرار التشغيل على المدى الواسع خاصة فى السرعات المنخفضة. يتم اشتقاق معادلة الخواص وذلك للمسار المغلق للتقدير الحسابي للسرعة والتى منها تحدد معاملات القانون التكيفى التى تناظر حدود استقرار النظام اعتمادا على معيار راوث. تم دراسة حساسية مراقب الفيض التكيفى لتغير مقاومة ملفات العضو الثابت. لذا تم عمل تقدير حسابي لمقاومة ملفات العضو الثابت بالتوازي مع السرعة اعتمادا على التيارات وذلك لحساب السرعة بدقة عند السرعات المنخفضة. تم توضيح العلاقة بين الخطأ فى التقدير الحسابى للسرعة وبين معاملات الكسب التكيفى. وقد تم تنفيذ هذا النظام المقترح معملياً باستخدام معالج الإشارات الرقمية، ويقدم البحث عرضا ومناقشة للنتائج التحليلية والمعملية. وقد تبين من نتائج البحث دقة نظام المراقبة المقترح ومتانته عند حالات التشغيل المختلفة مما يؤكد مدى فعالية هذا الأسلوب.

***Keywords***: Sensorless control, stability analysis, adaptive law design, low speed, stator resistance estimation.

## 1. INTRODUCTION

A great interest in the research community is given to develop high performance sensorless induction motor drives. The main approaches to eliminate the speed sensor are based on rotor slot harmonics, frequency signal injection and machine model [1]. Speed estimation utilizing rotor slot harmonics have the advantages of being independent of machine parameters. However, they need high precision measurements which increase the hardware/software complexity. Moreover, it may fail for certain slot combinations or skewing. The saliency based technique is machine specific and can not be applied to a standard machine [2]. Methods of speed estimation based on high frequency signal injection in stator voltages or currents may operate stably under zero-frequency condition, which occurs in regenerating mode at low speeds. However, they may increase losses and introduce torque ripples [1], [3].

Machine model based methods of speed estimation have found a great interest among different speed estimation methods for their simplicity. However, at low speeds, they are problematic. The main limitations arise from instability problems associated with most speed estimation schemes at low speeds

due to the change of machine parameters. The question that always arises is *to which extent the method is successful without deteriorating the dynamic performance of the drive during a wide speed range* [1].

Adaptive flux observer (AFO) is one of the machine model based methods of speed estimation of sensorless induction motor drives. Parameter variations, low-speed operation and the difficulty encountered in the design of the feedback gain and the adaptation mechanism are the most critical aspects affecting the accuracy and stability of this method. The characteristics of the speed estimation process are governed by how to deal with the aforementioned issues to guarantee the stability and tracking performance of the speed estimation in the sensorless drives during a wide range [4]-[13].

Many researches have been devoted to yielding better speed estimation of sensorless induction motor drives using AFO. However, there is a well known unstable region encountered at low speeds with regenerating loads. This unstable region of AFO can be reduced by proper design of both the observer feedback gain and adaptive law using several techniques. Remedies to cope with this instability problem are suggested in [5]. One of the techniques to design the observer feedback gain to deal with the problem is based on a decoupling control [6]. Another one utilized Routh-Hurwitz criterion [7]. Others are based on the linearized model of the speed adaptive full-order flux observer [8] or using Lyapunov theory [9]. Alternatively, improving the stability of the AFO by modifying the adaptive law is based on extensive numerical calculation of the current loci, and its stability is analyzed using a two-time-scale approach [10]. The ramp response characteristic of the speed estimator is used as design guidelines for the adaptation gains [9]. Stabilizing the Model Reference Adaptive System (MRAS)-based estimator for combined speed and stator resistance is achieved by adjusting the adaptive laws [11]. The instability problem for simultaneous estimation of rotor speed and stator resistance using average technique is solved [12]. In [13], all gain selections which give complete stability of AFO are obtained.

Recently, numerous attempts have been made to improve the performance of speed-sensorless induction motor drives, especially at low speeds, by identifying stator resistance together with speed. Stator resistance estimation is of utmost importance for accurate operation of sensorless induction motor drives in low speed region and also for minimizing the instability problems associated with AFO in this region. However, little interest has been given for stability analysis of combined speed and stator resistance estimators [8], [12], [14]. In addition, no criterion clarifies the relation between the adaptive gains and the identification error and how these gains affect both the convergence and steady state error of the speed estimator.

This paper is aimed at developing a stable AFO for speed estimation of sensorless induction motor drives. Design of the observer feedback gains is proposed to achieve the stability over a wide range of operation, especially in the low-speed region. The characteristic equation of the closed loop speed estimator is derived. Routh's stability criterion is applied to determine the gains of PI adaptation law corresponding to the marginal system stability. The designed AFO is remedied to be insensitive to parameter variations which have a major influence on accuracy and stability of low speed estimation. Therefore, a stator resistance estimation algorithm is used in parallel with rotor speed using Popov's hyper-stability theory. The boundedness of the identification error of the rotor speed and the relation between the identification error and the adaptive gains are clarified. To ensure the validity of the proposed approach, simulation and experimental results are presented at different operating conditions. Wide speed range estimation is achieved especially at very low speeds.

## 2. MATHEMATICAL MODELS FOR INDUCTION MOTOR AND ADAPTIVE FLUX OBSERVER

The block diagram for the proposed sensorless indirect field oriented (IFO) controlled induction motor drive is shown in Fig. 1.

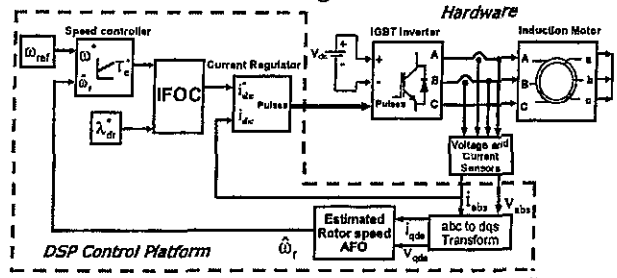


**Fig.1** Block diagram of sensorless indirect field oriented control system.

### 2.1. Dynamic Model of the Induction Motor

The induction motor can be described by the following dynamic equations in the synchronous reference frame, using stator current and rotor fluxes as state variables.

$$p\begin{bmatrix} i_s^e \\ \lambda_r^e \end{bmatrix} = \begin{bmatrix} a_{11} & a_{12} \\ a_{21} & a_{22} \end{bmatrix}\begin{bmatrix} i_s^e \\ \lambda_r^e \end{bmatrix} + \begin{bmatrix} B_{11} \\ 0 \end{bmatrix} v_s^e \quad (1)$$

$$\dot{x}^e = Ax^e + Bv_s^e \quad (2)$$

$$i_s^e = Cx^e$$

where,

$$x^e = \begin{bmatrix} i_s^e & \lambda_r^e \end{bmatrix}^T,\ i_s^e = \begin{bmatrix} i_{ds}^e & i_{qs}^e \end{bmatrix}^T,\ \lambda_r^e = \begin{bmatrix} \lambda_{dr}^e & \lambda_{qr}^e \end{bmatrix}^T$$

The electromechenical equation of the induction motor is given by

$$T_e = \frac{3}{2}\frac{P}{2}\frac{L_m}{L_r}\left(i_{qs}^e \lambda_{dr}^e - i_{ds}^e \lambda_{qr}^e\right) \quad (3)$$

### 2.2. Adaptive Flux Observer

The adaptive flux observer for estimating stator current and rotor flux can be constructed as follows;

$$\hat{x}^e = \hat{A}\hat{x}^e + Bv_s^e + K\left(\hat{i}_s^e - i_s^e\right)$$
$$\hat{i}_s^e = C\hat{x}^e \quad (4)$$

where K is the observer gain matrix.

The rotor speed is estimated using the adaptation mechanism based on Lyapunov stability theory [4], [8].

$$\hat{\omega}_r = K_p\varepsilon + K_I\int\varepsilon dt \quad (5)$$

where $K_P$ and $K_I$ are positive adaptation gains and the adaptive error signal $\varepsilon$ is

$$\varepsilon = e_{id}\hat{\lambda}_{qr} - e_{iq}\hat{\lambda}_{dr} \quad (6)$$

where

$$e_{id} = \hat{i}_{ds} - i_{ds} \text{ and } e_{iq} = \hat{i}_{qs} - i_{qs} \quad (7)$$

To obtain the observer error equation, subtract Eqn. (4) from Eqn. (2) yielding;

$$\dot{e} = \dot{x}^e - \dot{\hat{x}}^e = (A+KC)e + \Delta A\hat{x}^e$$
$$e_i = Ce \quad (8)$$

## 3. DESIGN OF THE FEEDBACK GAIN MATRIX

One of the main problems of designing AFO is determining the observer gain matrix K such that the error dynamics are asymptotically stable with sufficient speed of response. Eqn. (8) shows that the dynamic behavior of the error vector is determined by the eigenvalues of the matrix (A+KC). If the matrix (A+KC) is a stable matrix, the error matrix will converge to zero for any initial error vector. If the eigenvalues of the matrix (A+KC) are chosen in such a way that the dynamic behavior of the error vector is asymptotically stable and is adequately fast, the error vector will tend to zero with adequate speed. The first step in the pole placement design approach is to choose the locations of the desired closed loop poles. The most frequently used approach is choosing such poles based on experience in the root locus design, placing a dominant pair of the closed loop poles and choosing other poles so that they are far to the left of the dominant closed loop poles [7], [14].

The adaptive flux observer for stator current based on Eqn. (4) can be rewritten as,

$$p\hat{i}_s^e = (\hat{a}_{11} + K)\hat{i}_s^e + \hat{a}_{12}\hat{\lambda}_r^e + B_{11}v_s^e - Ki_s^e \quad (9)$$

The observer feedback gain matrix K is given by

$$K = \begin{bmatrix} K_1 & -K_2 \\ K_2 & K_1 \end{bmatrix} \quad (10)$$

$$\hat{a}_{11}+K = \begin{bmatrix} a_1 + K_1 & \omega_e - K_2 \\ -\omega_e + K_2 & a_1 + K_1 \end{bmatrix} \quad (11)$$

The characteristic equation of the AFO is

$$s^2 - 2(a_1+K_1)s + (a_1+K_1)^2 + (-\omega_e+K_2)^2 = 0 \quad (12)$$

So, the damping coefficient and the natural frequency can be obtained as follows,

$$\xi = \frac{-(a_1+K_1)}{\sqrt{(a_1+K_1)^2 + (-\omega_e+K_2)^2}} \quad (13)$$

$$\omega_n = \sqrt{(a_1+K_1)^2 + (-\omega_e+K_2)^2} \quad (14)$$

The eigenvalues of the observer are located into the left half of the S–plane compared to the eigenvalues of the system, so that the state of the observer converges rapidly.

$$s_{1,2} = (a_1+K_1) \pm j(-\omega_e+K_2) \quad (15)$$

## 4. ADAPTIVE LAW DESIGN

To find the values of the PI adaptive gains, we take Laplace transform of Eqn. (8):

$$se(s) = (A+KC)e(s) + \Delta A\hat{x}^e \quad (16)$$

$$e(s) = [sI - A - KC]^{-1}\Delta A\hat{x}^e \quad (17)$$

$$e_i(s) = Ce(s) = C[sI - A - KC]^{-1}\Delta A\hat{x}^e \quad (18)$$

$$\Delta A = A - \hat{A} = \begin{bmatrix} 0 & n \\ 0 & -1 \end{bmatrix} J\Delta\omega_r \quad (19)$$

$$e_i = C[sI - A - KC]^{-1}\begin{bmatrix} 0 & n \\ 0 & -1 \end{bmatrix} J\Delta\omega_r\hat{x}^e \quad (20)$$

The open loop transfer function between the adaptive error signal and the speed estimation error, assuming the observer gain K = 0, is given by Eqn. (21). All coefficients of Eqn. (21) are given in the appendix. The block diagram representing closed loop speed estimator is shown in Fig. 2.

$$G(s) = \frac{\varepsilon}{\Delta\omega} = \hat{\lambda}_{ro}^2 \frac{n_0 s^3 + n_1 s^2 + n_2 s + n_3}{s^4 + d_1 s^3 + d_2 s^2 + d_3 s + d_4} \quad (21)$$

Fig. 3 shows Root loci of G(s) at 150 rad/sec. As shown, the dominant poles are closer to the imaginary axis, giving slower error reduction. Variation of the dominant poles of G(s) is obtained at different rotor speeds as shown in Fig. 4. A Bode plot at various rotor speeds is shown in Fig. 5. It is obvious that the bandwidth of the speed estimator decreases with decreasing the speed.

The design of $K_P$ and $K_I$ is introduced to ensure stable operation. The following steps are followed for

determining the regions of $K_P$ and $K_I$ for both stable and unstable regions.

1. Derive transfer function of the closed loop speed estimator $\hat{\omega}_r/\omega_r$.

$$\frac{\hat{\omega}_r}{\omega_r} = \frac{G(s)(K_P + K_I/s)}{1+G(s)(K_P + K_I/s)} \qquad (22)$$

2. Applying Routh's stability criterion to find the conditions for marginal system stability.

It can be seen that the design of $K_P$ and $K_I$ is selected to ensure that all of the poles and zeros are located in the left hand side of the S-plane. This allows for the required fast response. Figure 6 shows reference, actual and estimated speeds, and speed estimation error during a step change of reference speed from 10 to 100 rad/sec at different values of PI gains. The results show how the choice of the correct values of PI adaptation gains affects the convergence of the estimated speed to the actual one.

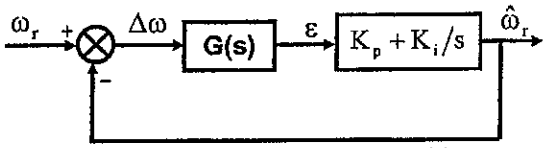


**Fig. 2** Block diagram representing closed loop speed estimator.

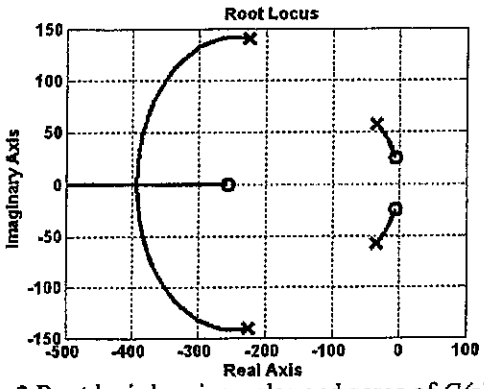


**Fig. 3** Root loci showing poles and zeros of *G(s)* at 150 rad/sec.

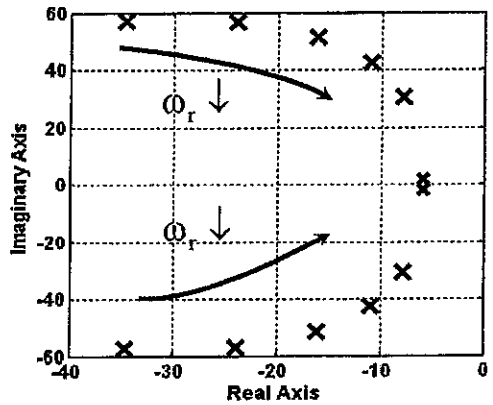


**Fig. 4** Dominant pole locations of *G(s)* at different rotor speeds 150, 115, 80, 50, 25 and 2 rad/sec.

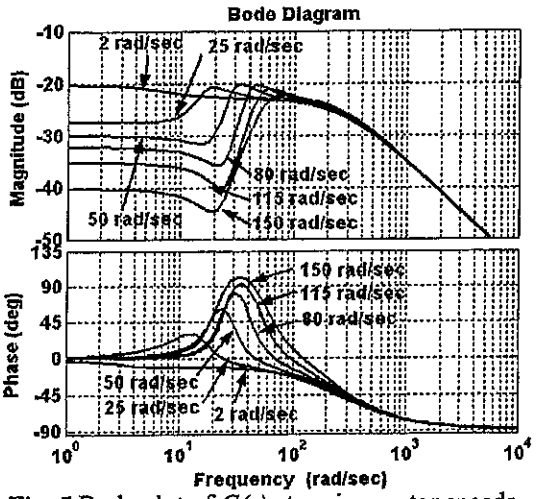


**Fig. 5** Bode plot of *G(s)* at various rotor speeds.

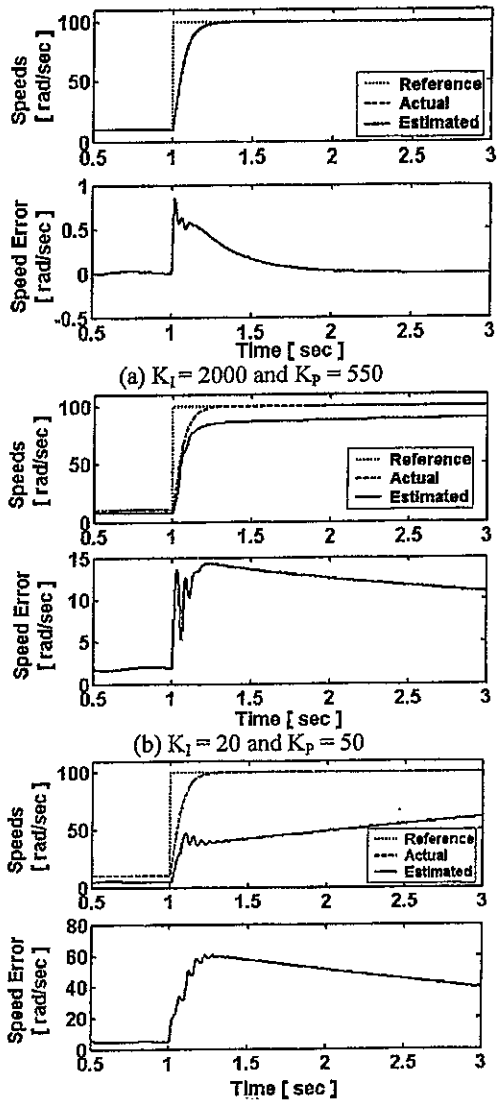


(a) $K_I = 2000$ and $K_P = 550$

(b) $K_I = 20$ and $K_P = 50$

(c) $K_I = 5$ and $K_P = 15$

**Fig. 6** Reference, actual and estimated speeds and speed estimation error during step change of speed reference from 10 to 100 rad/sec at different values of PI gains.

## 5. SENSITIVITY ANALYSIS

Practically, Parameter variations are unavoidable due to temperature rise and skin effects. The influence of parameter variations on the speed estimation is investigated by showing how parameter mismatch affects the speed estimation error. The sensitivity to stator resistance variations is firstly studied. Speed estimation error versus the stator resistance mismatch, at different rotor speeds equal to 0.5, 2, 5, and 100 rad/sec, is shown in Fig. 7. It can be seen that the speed estimation error dramatically increases at the low speed range. Also, stator resistance variations at high speeds have a very low speed error which can not exceed 1.1% at 200% $R_s$ mismatch. On the other hand, the speed estimation error has large values at very low speeds reaching 30% at 200% $R_s$ mismatch. The induced emf in the high speed range is high and the mismatch of the voltage drop across the stator resistance has a negligible effect on the speed estimation. At low speeds, the induced emf is very small and the mismatch of the voltage drop across the stator resistance has a serious influence on the speed estimation, which can lead the system into instability. In order to avoid this, the online stator resistance adaptation scheme has been applied.

On the other hand, variations of rotor resistance, leakage and mutual inductances do not cause instability problems in the speed estimation.

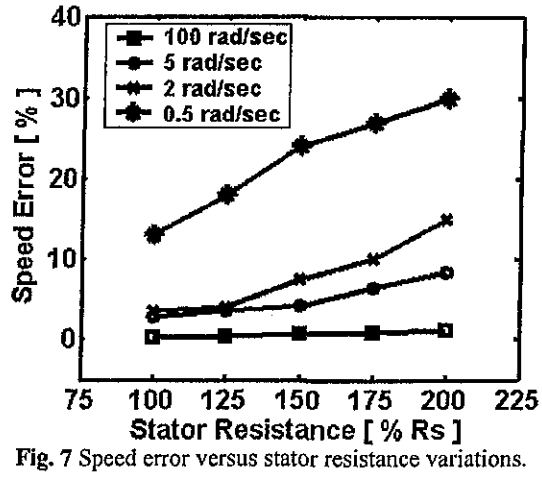


**Fig. 7** Speed error versus stator resistance variations.

## 6. SPEED AND STATOR RESISTANCE IDENTIFICATION SCHEMES

The aim of this section is to develop AFO which guarantees both stability and convergence of the estimated parameters.

If the rotor speed and stator resistance are considered as variable parameters, assuming no other parameter variations, the matrix $\Delta A$ is expressed as follows:

$$\Delta a_{11} = \frac{\Delta R_s I}{L_\sigma},\ \Delta a_{12} = \frac{\Delta \omega_r J}{\varepsilon},\ \Delta a_{21} = 0,\ \Delta a_{22} = \Delta \omega_r J \quad (23)$$

The error equation of the AFO is given by subtracting Eqn. (9) from Eqn. (1),

$$\dot{e}_i = a_{11}\left(\hat{i}_s^e - i_s^e\right) + \left(a_{11} - \hat{a}_{11}\right)\hat{i}_s^e + a_{12}\left(\lambda_r^e - \hat{\lambda}_r^e\right) + \left(a_{12} - \hat{a}_{12}\right)\hat{\lambda}_r^e + K\left(\hat{i}_s^e - i_s^e\right) \quad (24)$$

The estimation of rotor fluxes is constructed by an open loop observer represented by Eqn. (4) without the flux error, therefore $\lambda_r^e = \hat{\lambda}_r^e$;

Thus the error equation becomes,

$$\dot{e}_i = \left(a_{11} + K\right)e_i + \Delta a_{11}\hat{i}_s^e + \Delta a_{12}\hat{\lambda}_r^e \quad (25)$$

### 6.1. Stability of the Identification System

Popov's hyper-stability theory is applied to examine stability of the proposed identification system. This requires that the error system and the feedback system are derived so that the theory could be applied.

In the adaptive observer, using a speed identification error $\Delta\omega_r = \omega_r - \hat{\omega}_r$, a stator resistance identification error $\Delta R_S = R_S - \hat{R}_S$ and an error signal $e_i$, the error system from Eqn. (25) is written as:

$$\dot{e}_i = \left(a_{11} + K\right)e_i - W \quad (26)$$

The Popov's integral inequality of Eqn. (26) is written as follows [14], [15]:

$$\int_0^{t_0} e_i^T W\, dt \geq -\gamma^2,\ \gamma = \text{const.} \quad (27)$$

where $e_i$ is the input vector and $W = -z_1\Delta R_s - z_2\Delta\omega_r$, which represents the nonlinear block, is the output vector of the feedback block, and $\gamma$ is a finite positive constant which does not depend on $t_0$, and

$$z_1 = \left(1/L_\sigma\right)\hat{i}_s^e \quad (28)$$

$$z_2 = \left(J/\varepsilon\right)\hat{\lambda}_r^e \quad (29)$$

$$\int_0^{t_0} e_i^T W\, dt = \int_0^{t_0} e_i^T\left(-z_1\Delta R_s - z_2\Delta\omega_r\right)dt \quad (30)$$

*Substitution of Eqns. (28) and (29) in Eqn. (30)* yields,

$$\int_0^{t_0}\left(\frac{-e_i^T\Delta R_s}{L_\sigma}\hat{i}_s^e\right)dt + \int_0^{t_0}\left(\frac{-e_i^T\Delta\omega_r J}{\varepsilon}\hat{\lambda}_r^e\right)dt \geq -\gamma^2 \quad (31)$$

$$\int_0^{t_0}\left(-\frac{e_i^T\Delta R_s}{L_\sigma}\hat{i}_s^e\right)dt \geq -\gamma_1^2 \quad (32)$$

$$\int_0^{t_0}\left(\frac{-e_i^T\Delta\omega_r J}{\varepsilon}\hat{\lambda}_r^e\right)dt \geq -\gamma_2^2 \quad (33)$$

The validity of Popov's inequality of Eqn. (27) can be verified by means of the inequalities expressed by Eqns. (32) and (33), provided that the estimates of rotor speed and stator resistance can be obtained by Eqns. (34) and (35), respectively:

$$\hat{\omega}_r = K_\omega\int e_i^T J\hat{\lambda}_r^e dt \quad (34)$$

$$\hat{R}_s = K_R \int e_i^T i_s^e dt \qquad (35)$$

where $K_\omega$ and $K_R$ are adaptive gains.

An identification system for speed and stator resistance is shown in Fig. 8, which is constructed from a linear time-invariant forward block and a nonlinear time-varying feedback block. The system is hyper-stable if the forward block is positive real and the input and output of the nonlinear feedback block satisfy Popov's integral inequality. Block diagram of combined speed and stator resistance estimators is shown in Fig. 9.

### 6.2. Relation between Estimation Error and Adaptive Gains

This section will show the boundedness of the identification error of the rotor speed when the rotor speed is time-varying, and clarify the relation between the identification error and the adaptive gains. Considering the proportional gain $K_P$, Eqn. (34) can be rewritten as,

$$\dot{\hat{\omega}}_r = -K_{I\omega}\Delta\omega_r - K_{P\omega}\Delta\dot{\omega}_r \qquad (36)$$

from which;

$$\Delta\dot{\omega}_r = -\frac{K_{I\omega}}{1+K_{P\omega}}\Delta\omega_r - \frac{1}{1+K_{P\omega}}\dot{\omega}_r \qquad (37)$$

Now let the following conditions be satisfied:

$$\frac{K_{I\omega}}{1+K_{P\omega}} > 0 \qquad (38)$$

$$|\dot{\omega}_r| < \mu \text{ (const.)} \qquad (39)$$

The condition in Eqn. (38) is the necessary condition for the stability of the identifier which must always be satisfied. However, the condition in Eqn. (39) is the natural condition on the bound of the acceleration/deceleration determined by the mechanical load conditions.

The Lyapunov function must be determined in order to illustrate the relation between the estimation error and adaptive gains according to the Lyapunov stability theory.

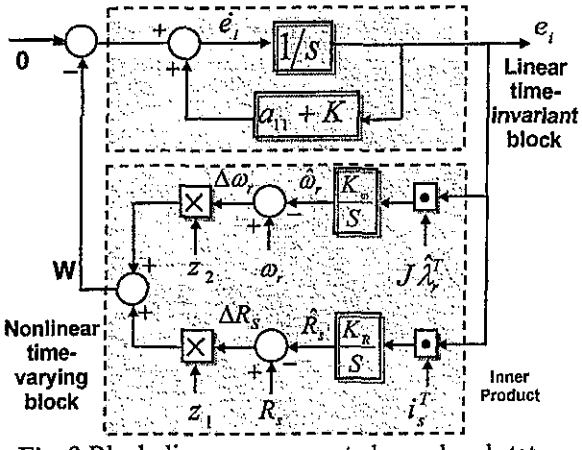


**Fig. 8** Block diagram represented speed and stator resistance identification system.

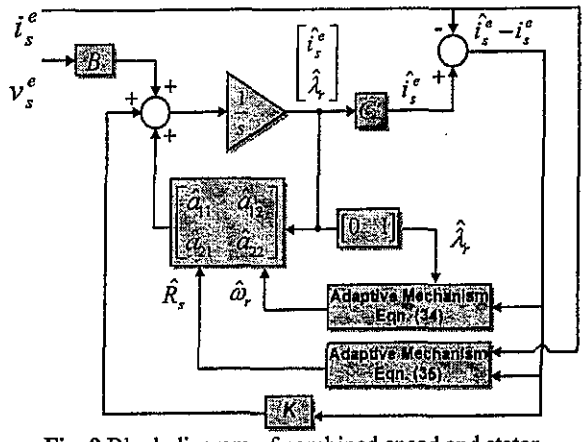


**Fig. 9** Block diagram of combined speed and stator resistance estimation.

The Lyapunov function V is chosen as;

$$V = \frac{1}{2}\Delta\omega_r^2 \qquad (40)$$

The time derivative of V can be expressed as;

$$\dot{V} = \Delta\omega_r \cdot \Delta\dot{\omega}_r \qquad (41)$$

According to Lyapunov stability theory, a system is stable when a positive definite Lyapunov function has a negative definite first derivative. The condition of Eqn. (41) being negative definite will be satisfied if $\dot{V} < 0$.

$$\dot{V} = -\frac{K_{I\omega}}{1+K_{P\omega}}|\Delta\omega_r|\left[|\Delta\omega_r| - d_{\max}\right] < 0 \qquad (42)$$

$$|\Delta\omega_r| < d_{\max} \qquad (43)$$

where;

$$d_{\max} = \frac{\mu}{K_{I\omega}} \qquad (44)$$

From the aforementioned results, it is clear that the bound of the identification error in Eqn. (44) is determined only by the integral gain $K_{I\omega}$ and is independent of the proportional gain $K_{P\omega}$. The proportional gain $K_{P\omega}$ contributes to the enhancement of the rate of convergence. This analysis is proved by Fig. 6 which shows the reference, actual and estimated speeds and speed estimation error during a step change of speed from 10 to 100 rad/sec at different adaptive gain values. As shown in the figure, the speed estimation error increases with decreasing the integral gain $K_{I\omega}$.

## 7. SYSTEM IMPLEMENTATION

The proposed algorithms of speed estimation are developed on a general purpose system development tools called *dSPACE*. The *dSPACE* tools consist of a *DS1102* hardware control board and a software interface program called *ControlDesk*. The main processing unit on the DS1102 control board is a Texas Instrument TMS320C31 DSP with 60 MHz

system clock. This control board is hosted by a personal computer for processing and downloading the control programs. In fact, *dSPACE* software tool is designed with an interface to SIMULINK by which it can convert a SIMULINK model to a machine code to be run on a DSP-based system. This greatly reduces the development and prototyping time for a variety of drive systems. On the other hand MATLAB/SIMULINK is provided with a Real Time Workshop (RTW) for communicating with data acquisition hardware such as the *dSPACE* control board *DS1102*. The control and estimation algorithms are developed on MATLAB/SIMULINK and then linked with real time system using the Built-In RTW. In this stage, the model is linked with the variables acquired from the drive system such as voltage and current signals via A/D input ports. All variables and subroutines are then correlated to the DSP environment, and, finally, an object file is created and downloaded to the DSP memory for real time operation. In the meantime any signal from the loaded program can be captured, stored or displayed using the *ControlDesk*. The schematic diagram of the experimental system is shown in Fig. 10.

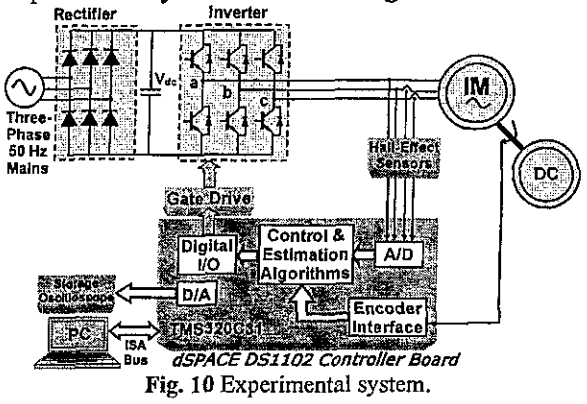


**Fig. 10** Experimental system.

## 8. RESULTS AND DISCUSSIONS

The experimental system, shown in Fig. 10, is built in laboratory to verify the accuracy of speed estimation based on AFO with stator resistance adaptation scheme. The parameters of the induction motor used as well as the controller gains are given in the appendix. Experimental results are presented to investigate the stability of the drive system at low speed operation. In addition the robustness of AFO to stator resistance mismatch and load torque disturbances is also investigated. Figure 11 shows the estimated speed during zero speed operation with initial +20% $R_s$ mismatch in the speed observer under light load of 20% of the rated value (1.5 N.m). As shown, there exists a substantial speed estimation error. Activation of stator resistance adaptation scheme is turned on at $t = 3$ *sec*. It is clear that the stator resistance estimator quickly removes the initial stator resistance error and consequently, eliminates the large speed estimation error. A considerable reduction of the speed error is observed with stator resistance adaptation due to +20% initial $R_s$ mismatch in the observer.

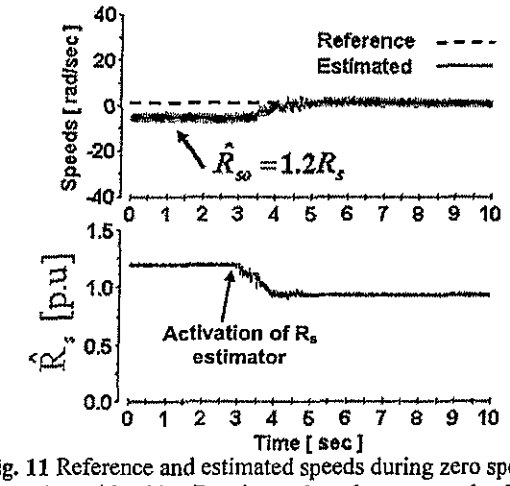


**Fig. 11** Reference and estimated speeds during zero speed operation with +20% $R_s$ mismatch under constant load of 20% of the rated value. Stator resistance adaptation is activated at $t = 3$ *sec.*

The drive system is also tested during dynamic performance. Figures 12 and 13 show the reference, actual and estimated speeds during very low speed reversal from 3 to -3 rad/sec and from 1 to -1 rad/sec, respectively under constant load of approximately 50% of the rated value. As shown, a good agreement between the actual and estimated speeds is achieved. The bandwidth of the speed observer decreases with decreasing the reference speed as shown in a Bode plot of Fig. 5. This consideration is confirmed by Figs. 12 and 13 which show the reference, actual and estimated speeds during a set of speed reversal. However, it should be noted that the lower speed reference the higher the time needed for speed reversal, because of the reduction of the speed bandwidth of the observer at decreasing speed references.

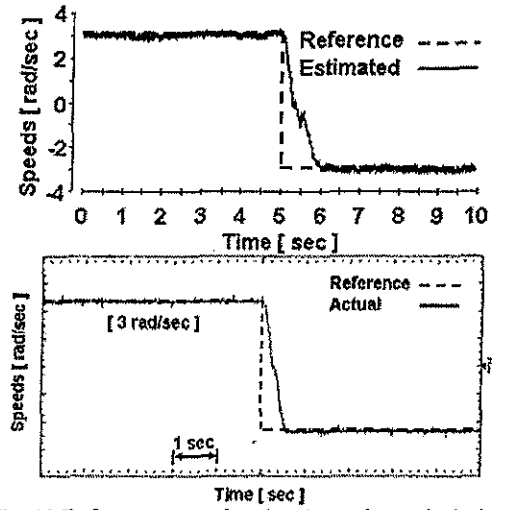


**Fig. 12** Reference, actual and estimated speeds during speed reversal at 3 rad/sec with stator resistance adaptation under constant load of 50% of the rated value.

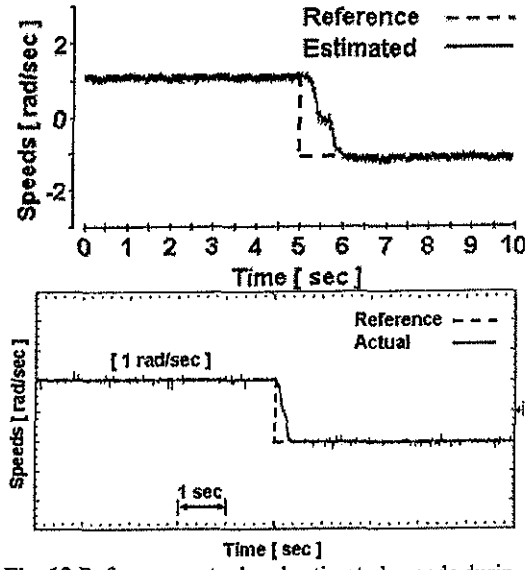


**Fig. 13** Reference, actual and estimated speeds during speed reversal at 1 rad/sec with stator resistance adaptation under constant load of 50% of the rated value.

Figure 14 shows the reference, actual and estimated speeds during zero speed operation with a sudden load change from light load (20%) to the rated value. It is obvious that the estimated speed tracks correctly the actual one. This confirms the robustness of the speed observer to load disturbances. The rotor speed and stator resistance are estimated by stable observers, therefore the proposed observers confront no problem in the low speed region. Furthermore, the algorithms of parallel speed and stator resistance identification scheme are characterized by their simplicity and small computation time.

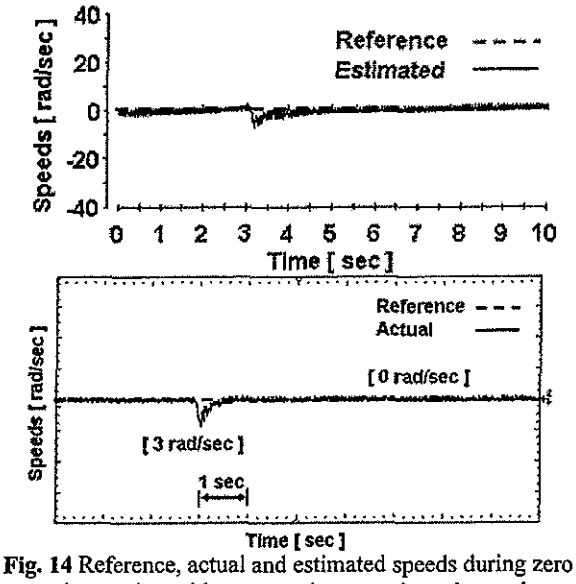


**Fig. 14** Reference, actual and estimated speeds during zero speed operation with stator resistance adaptation under a sudden load change from 20% to the rated value at $t$ =3 sec.

The IFO controller is also tested for the operation in the field weakening region. Fig. 15 shows reference, actual and estimated speeds during starting and reversing operation at 250 rad/sec under constant load of approximately 50% of the rated value. This Figure shows that a good agreement between the estimated and actual speeds in the field weakening region is achieved. Simulation and experimental results prove the ability of the AFO to provide an accurate speed estimate over a wide speed range from very low speed until high values beyond the rated speed. Moreover, the designed AFO is insensitive to stator resistance variations and is robust to a sudden load change.

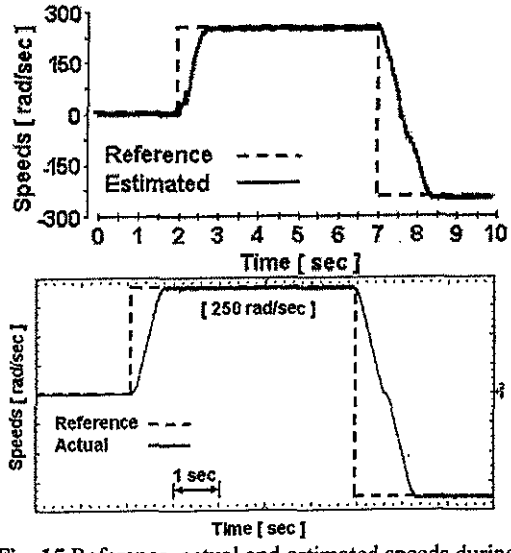


**Fig. 15** Reference, actual and estimated speeds during speed reversal at 250 rad/sec (field weakening region) under constant load of 50% of the rated value.

## 9. CONCLUSION

A design strategy for both feedback gains and adaptation gains of AFO, to guarantee the stability and tracking performance of the speed estimation in the sensorless drives, has been presented. The values of the adaptive law parameters corresponding to the marginal system stability have been determined using Routh's criterion. The rotor speed and stator resistance have been estimated by stable observers; therefore, they confront no problem in the low speed region. It has been made obvious that the bound of the identification error has been determined only by the integral gain and is independent of the proportional gain. The proportional gain contributes to the enhancement of the rate of convergence. The drive system has been tested during different operating conditions including dynamic performance, zero speed operation and field weakening operation. Very low speed sensorless operation and also zero speed have been investigated by the proposed AFO with online stator resistance adaptation scheme

without losing stability. Simulation and experimental results prove the ability of the AFO to provide an accurate speed estimate over a wide speed range from very low speed until high values beyond the rated speed. Moreover, the designed AFO is insensitive to stator resistance variations and is robust to a sudden load change. The results confirm the efficacy and the validity of the proposed approach for sensorless induction motor drives.

## 10. REFERENCES


[1] J. Holtz, "Sensorless Control of Induction Motor Drives", IEEE Proceedings, Vol. 90, No. 8, August 2002, pp. 1359-1394.

[2] C. S. Staines, C. Caruana, G. M. Asher, and M. Sumner, "Sensorless Control of Induction Machines at Zero and Low Frequency Using Zero Sequence Currents", IEEE Transactions on Industrial Electronics, Vol. 53, No. 1, February 2006, pp. 195- 206.

[3] M. Hinkkanen, V. M. Leppanen, and J. Luomi, " Flux Observer Enhanced With Low-Frequency Signal Injection Allowing Sensorless Zero-frequency Operation of Induction Motors", IEEE Transactions on Industry Applications, Vol. 41, No. 1, January/February 2005, pp. 52-59.

[4] J. Maes and J. A. Melkebeek, "Speed-Sensorless Direct Torque Control of Induction Motors Using an Adaptive Flux Observer", IEEE Transactions on Industry Applications, Vol. 36, No. 3, May/June 2000, pp. 778-785.

[5] L. Harnefors, "Instability Phenomena and Remedies in Sensorless Indirect Field Oriented Control", IEEE Transactions on Power Electronics, Vol. 15, No. 4, July 2000, pp. 733-743.

[6] S. Suwankawin and S. Sangwongwanich, "A Speed-Sensorless IM Drive With Decoupling Control and Stability Analysis of Speed Estimation", IEEE Transactions on Industrial Electronics, Vol. 49, No. 2, April 2002, pp. 444-455.

[7] H. Kubota, I. Sato, Y. Tamura, K. Matsuse, H. Ohta, and Y. Hori, "Regenerating-Mode Low-Speed Operation of Sensorless Induction Motor Drive with Adaptive Observer", IEEE Transactions on Industry Applications, Vol. 38, No. 4, July/August 2002, pp. 1081-1086.

[8] M. Hinkkanen, "Analysis and Design of Full-Order Flux Observers for Sensorless Induction Motors", IEEE Transactions on Industrial Electronics, Vol. 51, No. 5, October 2004, pp.1033- 1040.

[9] S. Suwankawin and S. Sangwongwanich, "Design Strategy of an Adaptive Full-Order Observer for Speed-Sensorless Induction-Motor Drives-Tracking Performance and Stabilization", IEEE Transactions on Industrial Electronics, Vol. 53, No. 1, February 2006, pp. 96- 119.

[10] H. Tajima, G. Guidi, and H. Umida, "Consideration about Problems and Solutions of Speed Estimation Method and Parameter Tuning for Speed-Sensorless Vector Control of Induction Motor Drives", IEEE Transactions on Industry Applications, Vol. 38, No. 5, September/October 2002, pp. 1282-1289.

[11] M. Rashed and A. F. Stronach, "A Stable Back-EMF MRAS-Based Sensorless Low Speed Induction Motor Drive Insensitive to Stator Resistance Variation", IEE Proceeding Electric Power Applications, Vol. 151, No. 6, November 2004, pp. 685-693.

[12] M. Saejia and S. Sangwongwanich, "Averaging Analysis Approach for Stability Analysis of Speed-Sensorless Induction Motor Drives With Stator Resistance Estimation", IEEE Transactions on Industrial Electronics, VOL. 53, NO. 1, February 2006, pp. 162-177.

[13] L. Harnefors, M. Hinkkanen, "Complete Stability of Reduced-Order and Full-Order Observers for Sensorless IM Drives", IEEE Transactions on Industrial Electronics, Vol. 55, No. 3, March 2008, pp. 1319-1329.

[14] H. M. Kojabadi, L. Chang, and R. Doraiswami, "A MRAS-Based Adaptive Pseudoreduced-Order Flux Observer for Sensorless Induction Motor Drives", IEEE Transactions on Power Electronics, Vol. 20, No. 4, July 2005, pp. 930 - 938.

[15] M. S. Zaky, M. M. Khater, S. S. Shokralla, and H. A. Yasin, "Wide Speed Range Estimation with Online Parameter Identification Schemes of Sensorless Induction Motor Drives", Accepted (October 14, 2008) for Publication In Transactions On Industrial Electronics.

[16] S. Maiti, C. Chakraborty, Y. Hori, M. C. Ta, "Model Reference Adaptive Controller-Based Rotor Resistance and Speed Estimation Techniques for Vector Controlled Induction Motor Drive Utilizing Reactive Power", IEEE Transactions on Industrial Electronics, Vol. 55, No. 2, Feb 2008, pp. 594-601.

[17] M. Barut, S. Bogosyan, and M. Gokasan, "Experimental Evaluation of Braided EKF for Sensorless Control of Induction Motors", IEEE Transactions on Industrial Electronics, Vol. 55, No. 2, February 2008, pp. 620-632.


## 11. APPENDIX

### A. List of symbols

| | |
|---|---|
| $L_m$ | Magnetizing inductance |
| $L_s$ | Stator leakage inductance |
| $L_r$ | Rotor leakage inductance |
| $R_s$ | Stator resistance |

| | |
|---|---|
| $T_r$ | Rotor time constant |
| $\omega_r$ | Actual Rotor speed |
| $\hat{\omega}_r$ | Estimated Rotor speed |
| $L_\sigma$ | Leakage coefficient |
| $i_s^e=[i_{ds}^e \;\; i_{qs}^e]^T$ | Actual Stator current vector |
| $\hat{i}_s^e=[\hat{i}_{ds}^e \;\; \hat{i}_{qs}^e]^T$ | Estimated Stator current vector |
| $\lambda_r^e=[\lambda_{dr}^e \;\; \lambda_{qr}^e]^T$ | Actual rotor flux vector |
| $\hat{\lambda}_r^e=[\hat{\lambda}_{dr}^e \;\; \hat{\lambda}_{qr}^e]^T$ | Estimated rotor flux vector |
| $v_s^e=[v_{ds}^e \;\; v_{qs}^e]^T$ | Stator voltage vector |

**B. Induction Motor Model**

The induction motor model in synchronous reference frame in terms of stator currents and rotor fluxes can be written as;

$$pi_{ds}^e = a_1 i_{ds}^e + \omega_e i_{qs}^e + a_2\lambda_{dr}^e + a_3\lambda_{qr}^e + bv_{ds}^e$$

$$pi_{qs}^e = a_1 i_{qs}^e - \omega_e i_{ds}^e + a_2\lambda_{qr}^e + a_3\lambda_{dr}^e + bv_{qs}^e$$

$$p\lambda_{qr}^e = -\omega_s\lambda_{dr}^e + a_5\lambda_{qr}^e + a_4 i_{qs}^e$$

$$p\lambda_{dr}^e = \omega_s\lambda_{qr}^e + a_5\lambda_{dr}^e + a_4 i_{ds}^e$$

$$I=\begin{bmatrix}1 & 0\\ 0 & 1\end{bmatrix},\quad J=\begin{bmatrix}0 & -1\\ 1 & 0\end{bmatrix}$$

$$a_{11}=a_1 I-\omega_e J,\; a_{12}=a_2 I+a_3 J,\; a_{21}=a_4 I,$$

$$a_{22}=a_5 I+\omega_s J,\; \omega_s=\omega_e-\omega_r$$

$$a_1=-\left(\frac{R_s}{L_\sigma}+\frac{L_m^2}{L_r T_r L_\sigma}\right),\; a_2=\frac{L_m}{L_r T_r L_\sigma},\; a_3=\frac{L_m}{L_r L_\sigma}\omega_r$$

$$a_4=\frac{L_m}{T_r},\; a_5=\frac{-1}{T_r},\; B_{11}=bI,\; b=\frac{1}{L_\sigma},\; C=[I \;\; 0]$$

$$L_\sigma=L_s-\frac{L_m^2}{L_r},\; T_r=\frac{L_r}{R_r},\; \varepsilon=\frac{L_m}{L_r T_r L_\sigma},\; n=\frac{L_m}{L_r L_\sigma}$$

**C. Induction motor parameters:-**

**Table I** Induction motor parameters

| | | | |
|---|---|---|---|
| Rated power (w) | 250 | $R_s$ (p.u) | 0.0658 |
| Rated voltage (volt) | 380 | $R_r$ (p.u) | 0.0485 |
| Rated current (Amp.) | 1.5 | $L_s$ (p.u) | 0.6274 |
| Rated frequency (Hz) | 50 | $L_r$ (p.u) | 0.6274 |
| Number of poles | 4 | $L_m$ (p.u) | 0.5406 |
| Moment of Inertia J ($Kg.m^2$) | 0.000 7 | Torque (N.m) | 1.5 |

**Table II** Controller Parameters

| Speed controller | |
|---|---|
| Proportional gain | 0.7 |
| Integral gain | 0.01 |

**D. Coefficients of G(s) are;**

$$n_o = n$$

$$n_1 = na_1 + 2na_5 - a_2$$

$$n_2 = -na_5^2 - n\omega_s^2 - 2na_1a_5 + na_2a_4 + a_3\omega_s + a_2a_5 + a_1a_2 - a_3\omega_e$$

$$n_3 = na_1a_5^2 + na_1\omega_s^2 - na_2a_4a_5 + na_3a_4\omega_s - a_1a_3\omega_s - a_1a_2a_5 - a_2\omega_e\omega_s + a_3a_5\omega_e + a_4a_2^2 + a_4a_3^2$$

$$d_1 = -(2a_1 + 2a_5)$$

$$d_2 = a_1^2 + a_5^2 + \omega_s^2 + \omega_e^2 + 4a_1a_5 - 2a_2a_4$$

$$d_3 = 2a_2a_4a_5 + 2a_3a_4\omega_s - 2a_1a_5^2 - 2a_1\omega_s^2 - 2a_1^2a_5 + 2a_1a_2a_4 - 2a_5\omega_e^2 - 2a_3a_4\omega_e$$

$$d_4 = -2a_1a_2a_4a_5 - 2a_1a_3a_4\omega_s + a_1^2a_5^2 + a_1^2\omega_s^2 - 2a_2a_4\omega_e\omega_s + 2a_3a_4a_5\omega_e + \omega_e^2a_5^2 + \omega_s^2\omega_e^2 + a_4^2a_2^2 + a_4^2a_3^2$$